Short-range order in α-brass

L. Reinhard, B. Schönfeld, and G. Kostorz
Institut für Angewandte Physik, Eidgenössischen Technischen Hochschule Zürich, CH-8093 Zürich, Switzerland

W. Bührer
Laboratorium für Neutronenstreuung der Eidgenössischen Technischen Hochschule Zürich, c/o Paul Scherrer Institut, CH-5303 Würenlingen, Switzerland

(Received 11 August 1989)

A quenched equilibrium state of a ^{65}Cu–31.1 at. % Zn single crystal was investigated by elastic diffuse neutron scattering. The short-range order intensity showed maxima that could be related to the flat portions of the Fermi surface perpendicular to the ⟨110⟩ directions. Effective pair potentials V_{lmn} were determined from 71 short-range order parameters α_{lmn} obtained from a fit to the diffuse intensity. Furthermore, 40 linear displacement parameters were also extracted. A dominant V_{110} of $\sim$18 meV was obtained. Based on a Monte Carlo simulation, an ordered low-temperature phase Cu_3Zn with the DO_{23} structure and a critical temperature of $\sim$330 K is suggested.

I. INTRODUCTION

The binary system Cu-Zn (brass) has been the subject of many electron-theoretical investigations, often relating the stability of various phases with the electron concentration of the alloy such as Hume-Rothery rules (for a short outline see Ref. 1). Whereas the order-disorder transition β'-β is well documented,[2] only indirect indications of short-range order are known in the primary solid solution (α phase) extending up to 38 at. % Zn. Short-range order may have contributed in measurements of the specific heat,[3] the electrical resistivity,[4,5] the Zener relaxation,[6] and the Mössbauer spectrum.[7] There has been an early attempt by Keating[8] using neutron scattering to directly detect short-range order in the α phase, but it failed.

For a quantitative investigation of short-range order, diffuse neutron and x-ray scattering are well suited.[9–12] In the present investigation, neutron scattering was applied. In comparison with x rays, the coherent scattering contrast between Cu and Zn is considerably higher for neutrons (8% instead of 0.1%) and can be increased further (by a factor of 3.6) using the ^{65}Cu isotope. Furthermore, the reciprocal space close to the direct beam is often critical in a quantitative evaluation of short-range order (see, e.g., the discussion in Ref. 13), and is easily accessible with neutrons as measurements are possible in transmission. Inelastic scattering contributions can widely be suppressed, and form-factor variations are negligible.

From the short-range order scattering of a sample representing a state of thermodynamic equilibrium, effective pair potentials can be obtained by various techniques. These potentials might then be used to suggest low-temperature phases otherwise not easily accessible because of kinetic reasons. Furthermore, they offer a valuable comparison with electronic structure calculations, e.g., those based on the Korringa-Kohn-Rostoker coherent-potential approximation (KKR-CPA; see Ref. 1 and references therein).

II. THEORY

The elastic coherent scattering from a disordered alloy consists of one contribution from the mean lattice (Bragg scattering) and of another due to the deviations from this mean lattice (diffuse scattering, $I_{\rm diff}$). These deviations are caused either by local concentration fluctuations (short-range order scattering, $I_{\rm SRO}$) or by static displacements due to the atomic size effect [scattering from "small" displacements (linear approximation), $I_{\rm SE}$]:

$$I_{\rm diff}(\mathbf{Q})=I_{\rm SRO}(\mathbf{Q})+I_{\rm SE}(\mathbf{Q}) , \tag{1}$$

where $\mathbf{Q}$ is the scattering vector. In Laue units, these terms are given by[12]

$$I_{\rm SRO}(\mathbf{h})/I_{\rm Laue}=\sum_l\sum_m\sum_n \alpha_{lmn}\cos(\pi h_1 l)\cos(\pi h_2 m)\cos(\pi h_3 n) , \tag{2}$$

$$I_{\rm SE}(\mathbf{h})/I_{\rm Laue}=\sum_l\sum_m\sum_n [h_1\gamma^x_{lmn}\sin(\pi h_1 l)\cos(\pi h_2 m)\cos(\pi h_3 n)$$
$$+h_2\gamma^y_{lmn}\cos(\pi h_1 l)\sin(\pi h_2 m)\cos(\pi h_3 n)+h_3\gamma^z_{lmn}\cos(\pi h_1 l)\cos(\pi h_2 m)\sin(\pi h_3 n)] , \tag{3}$$

 ©1990 The American Physical Society

with $I_{\text{Laue}}=Nc_Ac_B(b_A-b_B)^2e^{-2M}$ (c_A and c_B are the atomic fractions, b_A and b_B the coherent scattering lengths for the components A and B of the alloy; e^{-2M} is the Debye-Waller factor and N the number of atoms in the beam). The mean lattice position $\mathbf{r}$ and the scattering vector $\mathbf{Q}$ are expressed by the unit vectors of the fcc and its reciprocal lattice, $\mathbf{a}_i$ and $\mathbf{a}_i^*$, respectively,

$$\begin{aligned}\mathbf{r}&=l(\mathbf{a}_1/2)+m(\mathbf{a}_2/2)+n(\mathbf{a}_3/2)\ ,\\ \mathbf{Q}&=h_1\mathbf{a}_1^*+h_2\mathbf{a}_2^*+h_3\mathbf{a}_3^*\ ,\end{aligned}\tag{4}$$

where l,m,n are integers and the h_i are continuous variables. The Warren-Cowley short-range order parameters α_{lmn} describe the deviation from a random arrangement of A and B atoms. The Fourier coefficients γ^i_{lmn} depend on the concentrations, coherent scattering lengths, and the relative average displacements in i direction of A-A and B-B pairs.

Whereas the short-range order scattering, I_{SRO}, has $Im3m$ symmetry—there is a zero gradient at 000, 100, $\frac{1}{2}\frac{1}{2}\frac{1}{2}$, $1\frac{1}{2}0$ positions, the "special points"[14]—the displacement scattering has $m3m$ point symmetry. I_{SRO} and I_{SE} are differently weighted with the coherent scattering lengths b_A and b_B. The larger the ratios $b_A/(b_A-b_B)$ and $b_B/(b_A-b_B)$, the larger the contribution of the linear displacement scattering in comparison with short-range order scattering.

In thermal equilibrium, the arrangement of the atoms in the alloy is determined by the interactions between the atoms. Considering only pairwise interactions V_{ij}^{nm} (i,j describe the atomic sites and n,m the atom type), the Hamiltonian H of a grandcanonical ensemble is of the Ising type,[15]

$$H=\tfrac{1}{4}\sum_{i\neq j}\sum V_{ij}S_iS_j+\Delta\mu\sum_i S_i\ ,\tag{5}$$

where $V_{ij}=\frac{1}{2}(V_{ij}^{AA}+V_{ij}^{BB}-2V_{ij}^{AB})$ is the effective pair potential and $\Delta\mu$ is a kind of chemical-potential difference. The occupation numbers S_i are $+1$ for B atoms and -1 for A atoms.

To determine the effective pair potentials V_{ij} from short-range order scattering, two methods were employed. (1) The high-temperature approximation of Clapp and Moss[15] yields

$$I_{\text{SRO}}(\mathbf{h})/I_{\text{Laue}}=C/[1+2c_Ac_B\tilde{V}(\mathbf{h})/(k_BT)]\ ,\tag{6}$$

where $\tilde{V}(\mathbf{h})$ is the Fourier transform of V_{ij}. For the normalization constant C a value of 1 was used (see Ref. 16 for a discussion of C). (2) The approximation-free inverse Monte Carlo method[17] is based on the fact that in thermodynamic equilibrium, observables weighted with a transition probability will not vary if many fluctuations are considered. In the present case, the observable considered was the number of B-B pairs in any given distance $\mathbf{r}$ which was modified in changing from one microscopic state to another by a virtual A-B interchange. This yields nonlinear equations for the V_{ij}, as the transition probability to another microscopic state itself is a function of the energy change due to the transition.

III. EXPERIMENTAL

A single crystal of α-brass was grown by the Bridgman technique using zone-refined, isotopically pure [99.2(2)%] ^{65}Cu and 99.9999% Zn. The sample used in the scattering experiment was cut by spark erosion, with a diameter of 9.9 mm and a height of 9.6 mm. Its Zn concentration as determined by chemical analysis was 31.1 at. %, with a homogeneity of better than 0.2 at. % over the sample length. The mosaic spread (full width at half maximum) for the 200 reflection was 1.6° (still convoluted with the instrumental resolution which was always clearly less than 1°).

The sample was homogenized at 1123 K for 170 h, aged at 473 K for 160 h in a sealed quartz tube under a high-purity argon atmosphere, and water quenched. This aging was chosen to assure that an equilibrium state was frozen in: The relaxation time at 473 K is $\sim$1000 s.[5]

The neutron scattering measurements were performed at the triple-axis spectrometer R5 at the Laboratorium für Neutronenstreuung in the elastic mode. One plane each of {100}, {110}, and {111} type was investigated using neutrons of a wavelength of 0.244 nm within a range of 0.5–2.3 for the magnitude of the scattering vector [in reciprocal lattice units, see Eq. (4)] and a wavelength of 0.415 nm for h ranging from 0.2 to 0.5. About 950 data points were measured in each plane with a mesh of $\Delta h\approx\frac{1}{30}$. Count rates were 1500–7000 counts per 5 min and 600–800 counts per 30 min for $\lambda=0.244$ and 0.415 nm, respectively. Harmonics were suppressed by pyrolytic graphite and a beryllium filter. The data were calibrated by measuring the incoherent scattering from a hollow vanadium cylinder of the same outer dimensions and alignment as the sample. These measurements were taken on a wider mesh ($\sim$120 data points).

For the evaluation, neutron cross sections σ and scattering lengths b were taken from Sears:[18] $\sigma_{\text{inc}}=0.40(5)$ barn, $\sigma_{\text{abs}}(2200\ \text{m/s})=2.17(3)$ barn, $b=10.61(19)$ fm for ^{65}Cu and $\sigma_{\text{inc}}=0.077(7)$ barn, $\sigma_{\text{abs}}(2200\ \text{m/s})=1.11$ barn, $b=5.680(5)$ fm for Zn. Only the value of $\sigma_{\text{inc}}=5.08(6)$ barn for vanadium is based on a private communication by Sears. After subtracting the background—typically 2–5 % of the scattered intensity, but up to 60% close to the direct beam—data were corrected for absorption and multiple scattering using the program DISCUS (Ref. 19) and a modified version for the case of a hollow cylinder. The ratio of multiple scattering to single scattering was 1.5 to 3%. The Debye-Waller factors $\exp(-\frac{1}{2}|\mathbf{Q}|^2\langle u^2\rangle)$ were calculated using mean square displacements, $\langle u^2\rangle$, of 0.0061 Å^2 and 0.0073 Å^2 for vanadium[20] and α-brass[21,22] containing 31.1 at. % Zn, respectively.

IV. RESULTS

Figures 1(a)–1(c) show the diffusely scattered intensity in the (001), (011), and (111) planes. The hatched areas around the Bragg positions which might be affected by the wings of the Bragg peaks, and close to the direct beam where the background is high, were excluded. Furthermore, within $\Delta h<0.1$, some inelastic (thermal

diffuse) scattering may still be included in the total intensity. The diffuse scattering intensity is strongly modulated, showing distinct maxima within the (001) plane, between the Bragg reflections, i.e., there is short-range order. These maxima are not located at the special Lifshitz points of high symmetry.

As pointed out by Moss,[23] maxima of diffuse scattering may also occur for $2\mathbf{k}_F^{uvw}$, $\mathbf{k}_F$ being the Fermi vector, if flat portions of the Fermi surface are present perpendicular to the $\langle uvw \rangle$ directions. Such flat portions across the $\langle 110 \rangle$ directions have been "imaged" by diffuse scattering in various copper alloys, like Cu-Au,[23,24] Cu-Pt,[25] Cu-Pd,[25] and Cu-Al.[26] These maxima are caused by a singularity in the static dielectric function, $\epsilon(\mathbf{Q})$, shielding the pure ion-ion interaction $\tilde{V}^0(\mathbf{Q})$. As seen in Eq. (6), minima in the effective pair interaction $\tilde{V}(\mathbf{Q})=\tilde{V}^0(\mathbf{Q})/\epsilon(\mathbf{Q})$ will lead to maxima in the short-range order scattering. Thus, it may be inferred that intersections of "anomalous surface portions" give rise to the fourfold maxima around the 110 position, as well as to the twofold maxima around the 100 position within the (001) plane, as illustrated in Fig. 1(d).

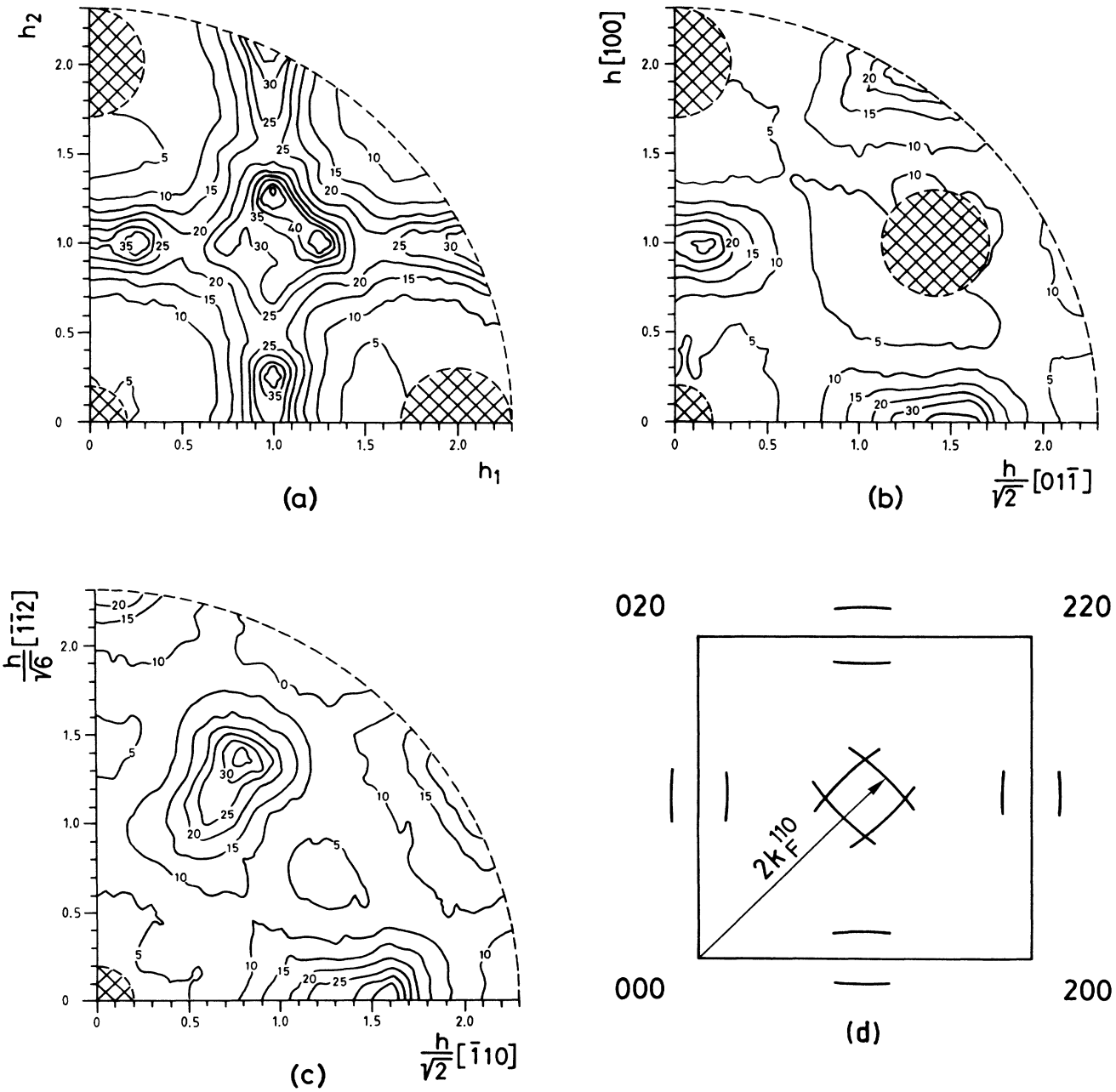

FIG. 1. Elastic diffuse scattering $I_{\text{diff}}(\mathbf{h})$ in 0.1 Laue units for (a) the (001), (b) the (011), and (c) the (111) plane. The relation between the maxima in short-range order scattering and the Fermi vector $|\mathbf{k}_F^{110}|$ is sketched for the (001) plane in (d).

Using the location of the maxima one obtains $|\mathbf{k}_F^{110}| = 1.38(2)$ Å^{-1} [this value was more precisely determined from the maxima in the short-range order scattering after separation of the displacement scattering whose influence is clearly visible in the different intensities of the maxima around the 110 position, Fig. 1(a)]. This value compares well with $|\mathbf{k}_F^{110}| = 1.40(2)$ Å^{-1} found in positron annihilation experiments for a Cu–30 at. % Zn alloy.[27] Coherent-potential approximation (CPA) calculations also yield a similar value of 1.41(1) Å^{-1} for the same concentration.[28]

To the scattered intensities, 71 α_{lmn} and 40 γ^i_{lmn} were fitted by a weighted least-squares procedure, a method introduced by Williams.[29] The data are listed in Tables I and II. The (underestimated) errors are based solely on counting statistics. Figure 2 compares the measured intensities, I_i^{meas} [the data of the (001) plane were symmetrized], with those recalculated from the Fourier coefficients of Tables I and II, I_i^{calc}. A good agreement is found as seen in the weighted R value and x^2 of the fit, with 0.088 and 4.1, respectively. These terms are defined as

$$R = \left[\sum_i w_i (I_i^{\text{meas}} - I_i^{\text{calc}})^2 \Big/ \left[\sum_i w_i (I_i^{\text{meas}})^2 \right] \right]^{0.5}$$

with w_i = weight, and

$$x^2 = \sum_i w_i (I_i^{\text{meas}} - I_i^{\text{calc}})^2 \Big/ (p - n - 1)$$

with n = number of fitted Fourier coefficients to the p intensities. Whereas the position of the sharp maxima around the 110 position is well reproduced, their measured intensity is still somewhat higher than the calculated values. This might be an indication that even more Fourier coefficients are required. The present system of equations, however, becomes unstable with more than 90 α_{lmn}.

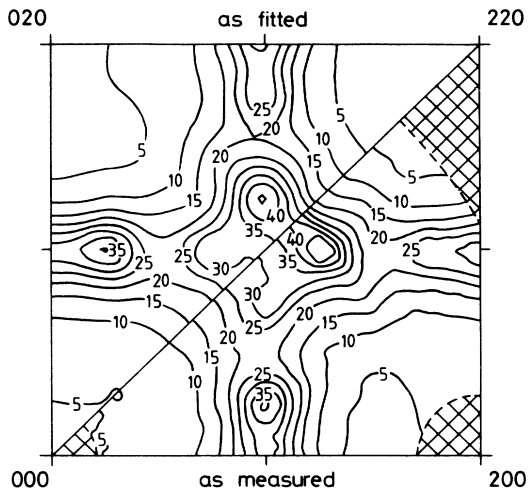

FIG. 2. Measured and fitted diffuse scattering $I_{\text{diff}}(\mathbf{h})$ in 0.1 Laue units for the (001) plane.

A. Short-range order

The quality of a diffuse scattering experiment is sometimes simply judged by the deviation of α_{000} from its theoretical value of 1; in the present case, a deviation of 8% is observed. Considering the uncertainties of the input parameters in the data evaluation, it is found that the

TABLE I. Warren-Cowley short-range order parameters α_{lmn}.

lmn	α_{lmn}	lmn	α_{lmn}	lmn	α_{lmn}
000	1.0831(31)	620	0.0050(4)	822	0.0007(4)
110	−0.1373(9)	541	0.0041(4)	743	0.0003(3)
200	0.1490(11)	622	0.0024(5)	750	−0.0004(4)
211	0.0196(7)	631	0.0013(3)	831	−0.0004(3)
220	0.0358(8)	444	−0.0099(7)	662	0.0002(4)
310	−0.0404(5)	543	0.0028(3)	752	0.0007(3)
222	−0.0077(9)	550	−0.0036(6)	840	0.0006(4)
321	−0.0036(4)	710	−0.0028(5)	833	−0.0001(4)
400	0.0296(11)	640	−0.0001(4)	910	−0.0010(4)
330	−0.0134(7)	552	−0.0006(4)	842	0.0001(3)
411	0.0141(6)	633	0.0006(4)	655	−0.0006(4)
420	0.0050(5)	721	−0.0013(4)	761	−0.0013(3)
332	−0.0005(5)	642	−0.0011(3)	921	−0.0005(3)
422	−0.0050(6)	730	−0.0008(4)	664	−0.0003(4)
431	0.0068(3)	651	−0.0002(3)	754	0.0006(3)
510	−0.0107(5)	732	0.0006(3)	851	−0.0004(3)
521	−0.0019(4)	800	0.0060(9)	930	−0.0003(4)
440	−0.0050(7)	554	0.0006(4)	763	−0.0008(3)
433	0.0038(4)	741	0.0007(3)	932	−0.0004(2)
530	−0.0066(4)	811	−0.0007(5)	844	0.0002(4)
442	−0.0084(5)	644	−0.0016(4)	770	0.0000(5)
600	0.0130(13)	820	0.0020(4)	853	−0.0008(3)
532	−0.0003(3)	653	−0.0005(3)	941	0.0003(3)
611	0.0023(5)	660	0.0007(7)		

TABLE II. Linear displacement parameters γ^i_{lmn}, $i=x,y,z$.

lmn	γ^x_{lmn}	γ^y_{lmn}	γ^z_{lmn}
110	0.0314(4)		
200	−0.0187(11)		
211	−0.0154(6)	−0.0016(3)	
220	0.0144(6)		
310	0.0029(6)	−0.0006(4)	
222	0.0098(5)		
321	−0.0018(4)	−0.0081(4)	0.0011(3)
400	−0.0087(11)		
330	0.0048(5)		
411	−0.0010(6)	−0.0001(3)	
420	−0.0035(4)	0.0030(4)	
332	−0.0025(4)	0.0006(3)	
422	−0.0004(4)	0.0022(3)	
431	0.0003(3)	−0.0019(3)	0.0010(2)
510	0.0001(4)	−0.0018(4)	
521	0.0006(3)	−0.0016(3)	−0.0004(3)
440	0.0003(4)		
433	−0.0008(4)	0.0001(3)	
530	−0.0005(4)	−0.0001(4)	
442	0.0012(4)	−0.0002(3)	
600	−0.0015(8)		
532	−0.0009(3)	−0.0004(3)	−0.0006(3)

possible error in the elastic scattering length for ^{65}Cu is dominant, leading to an uncertainty of 8% in α_{000} (and also in the other α_{lmn}). The next important uncertainty (amounting to 5%) is introduced by σ_{inc} of ^{65}Cu, affecting only α_{000}. Thus, from these two possible sources of error, the measured deviation of α_{000} from 1 is acceptable.

The short-range order parameter α_{110} is negative, indicating a preference for Zn atoms as nearest neighbors of Cu atoms. This preference, however, is not as pronounced as it could be: Short-range order is not strongly developed. Consistently, the experimental value of α_{110} amounts to only about one-third of its lower limit of $(1-c_{\text{Cu}}^{-1})$.

Another feature of the parameters α_{lmn} is notable. All α_{2n00} are positive while the $\alpha_{(2n-1)10}$ are negative. This indicates that atoms of the same kind will form chains along ⟨100⟩ directions. This tendency is already visible in Fig. 3 where the intensity maxima are found to be elongated along ⟨100⟩ directions. Much stronger intensity ridges related to similar arrangements were observed in Au_4Mn.[30]

B. Crystal modeling

The aim for modeling a short-range ordered crystal by computer simulations is twofold: (1) to "visualize" the short-range ordered state and (2) to look for special configurations related to long-range ordered structures. An fcc model crystal with 13 104 atoms was fitted to the experimental short-range order parameters of Table I. It was possible to model crystals showing α_{lmn} which were all within the statistical error bars (Table I) of the experimental ones. A (001) plane of such a modeled crystal is shown in Fig. 4, along with one of a random arrangement

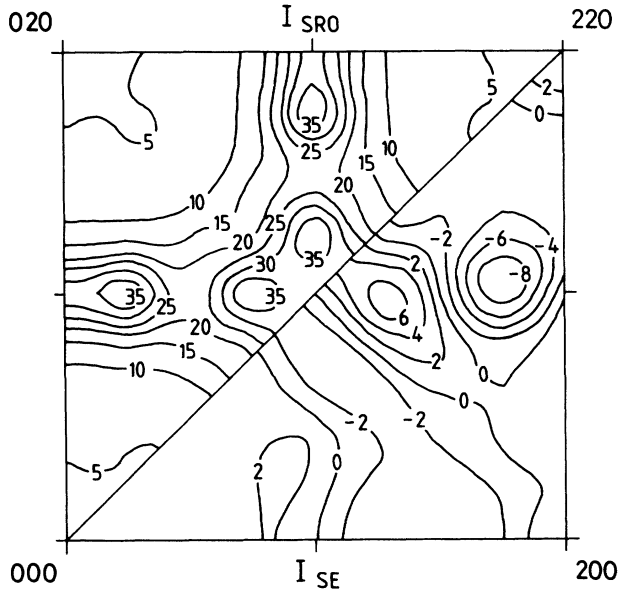

FIG. 3. Short-range order scattering $I_{\text{SRO}}(\mathbf{h})$ and linear displacement scattering $I_{\text{SE}}(\mathbf{h})$ in 0.1 Laue units for the (001) plane.

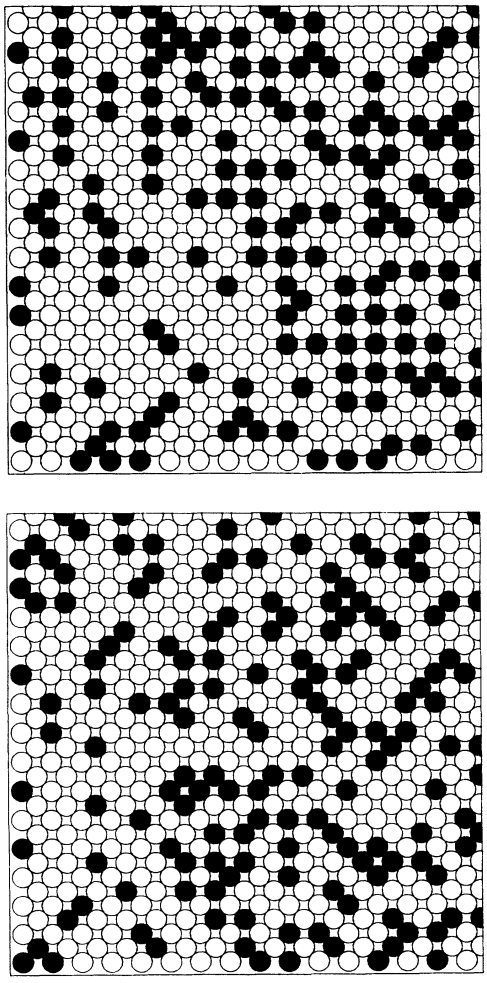

FIG. 4. (001) plane of a modeled short-range ordered alloy (a) and for a random arrangement with identical composition (b).

TABLE III. Abundance (%) of chains of Zn atoms of length L along ⟨100⟩ directions, normalized to the total number of Zn atoms, for the short-range ordered alloy and for a random arrangement.

	Abundance (%)	
L	Random	Short-range ordered
1	10.8	4.4
2	44.3	42.6
3	14.0	17.6
4	4.3	7.3
5	1.4	3.8

($\alpha_{lmn\neq 000}=0$) and identical composition for comparison. Chains of Zn atoms along ⟨100⟩ directions are clearly visible in the short-range ordered crystal. Table III quantifies this impression by listing the abundance of chains of length L for a random arrangement and for the short-range ordered alloy: Whereas the number of smaller chains decreases, the number of larger ones increases on ordering.

A systematic way of detecting elements of a long-range ordered structure is possible by an analysis of the Clapp configurations[31] which describe the arrangement of the alloying partners within the nearest-neighbor shell. Table IV shows the main items of such an analysis. Once again, the data of a random arrangement help to indicate the tendencies. Considering the case of Zn atoms around a Cu atom, the planar $C16$ and the tetrahedral $C17$ configurations show a distinct increase upon ordering. Because of the nonstoichiometry of the alloy investigated, compatible configurations are of equal importance: Considering also configurations with additional Zn atoms (Clapp configuration numbers of Table IV larger than 16 or 17), there is always an increase with ordering, whereas a decrease soon occurs in replacing Zn atoms by Cu atoms (numbers smaller than 16 or 17). As $C16$ and $C17$ are basic structure elements of the $L1_2$ superstructure and the antiphase boundaries therein, respectively, the abundance analysis thus indicates a Cu–25 at.% Zn superstructure of the $L1_2$ type with (presumably) periodic antiphase boundaries.

TABLE IV. Abundance of some Clapp configurations for the first coordination shell and the case of Zn atoms around a Cu atom. Data are given for the short-range ordered alloy and a random arrangement.

	Configuration abundance (%)	
Configuration	Random	Short-range ordered
$C16$	0.2	1.9
$C7$	1.2	3.4
$C3, C4$	4.2	2.9
$C34$	0.5	3.8
$C58, C60, C61$	0.4	2.2
$C17$	0.3	2.1
$C8$	2.5	5.1
$C3, C5$	8.4	5.2
$C35, C37$	1.1	4.9
$C62, C63, C65, C66$	1.1	3.6

C. Effective pair interactions

To determine the effective pair potentials V_{lmn} by the inverse Monte Carlo method, crystals containing 32 768 atoms were modeled. Virtual interchanges of A and B atoms were considered for all A and B atoms being nearest neighbors. This resulted in ~90 000 virtual site changes. Twenty potentials were then determined; they are listed in Table V. The errors were estimated from the variations found when comparing three separately modeled crystals, all of them consistent with the experimental short-range order parameters, and from the uncertainties resulting from the statistical errors in α_{lmn}. Both error estimates are of the same order of magnitude.

In using the Clapp-Moss approximation, two procedures were followed. First, 20 effective pair potentials were fitted to the short-range order scattering after subtracting the displacement scattering: $I_{\text{diff}}-I_{\text{SE}}-(\alpha_{000}-1)$. Secondly, effective pair interactions were obtained by Fourier transformation, using the calculated short-range order scattering (Table I) and Eq. (6). The resulting errors are based on the uncertainty in α_{lmn}.

Table V shows that the nearest-neighbor pair potential, V_{110}, is dominant. Though $V_{110}/(k_BT)\approx 0.46$, a similar value is obtained in the high-temperature approximation as in the approximation-free inverse Monte Carlo method. The other V_{lmn} also agree well within the various evaluations.

There is no slower decrease of the V_{lmn} along ⟨110⟩ directions, as one might expect from the Friedel potential[32] and the "flatness" of the Fermi surface perpendicular to the ⟨110⟩ directions. A similar effect was observed in Cu-Al, where a $2k_F$ singularity was seen in the diffuse

TABLE V. Effective pair potentials V_{lmn} in meV as determined by the inverse Monte Carlo method (IMC) and the Clapp-Moss approximation using a Fourier transformation (FT) and a least-squares fitting procedure (LSF).

lmn	V_{lmn}^{IMC}	V_{lmn}^{FT}	V_{lmn}^{LSF}
000		37.6(5)	29.8(5)
110	18.6(3)	18.1(2)	15.5(3)
200	−6.6(3)	−7.4(1)	−7.8(3)
211	−1.3(2)	−1.4(2)	−1.6(2)
220	−0.1(2)	−0.3(2)	−0.4(2)
310	0.5(3)	0.2(3)	0.2(2)
222	1.2(2)	0.8(2)	0.4(2)
321	0.9(1)	0.6(1)	0.3(1)
400	0.4(5)	0.2(5)	0.0(2)
330	0.6(1)	0.4(1)	0.2(1)
411	0.7(2)	0.5(2)	0.3(1)
420	0.9(1)	0.7(2)	0.4(1)
332	0.8(1)	0.6(2)	0.2(1)
422	0.4(1)	0.1(3)	−0.1(1)
431	0.2(1)	0.0(1)	−0.1(1)
510	0.1(3)	−0.3(2)	−0.1(1)
521	0.2(1)	−0.1(1)	0.0(1)
440	0.4(1)	0.2(2)	0.4(1)
433	0.3(1)	0.3(1)	0.1(1)
530	0.5(1)	0.2(1)	0.3(1)
442	0.3(1)	0.1(2)	0.2(1)

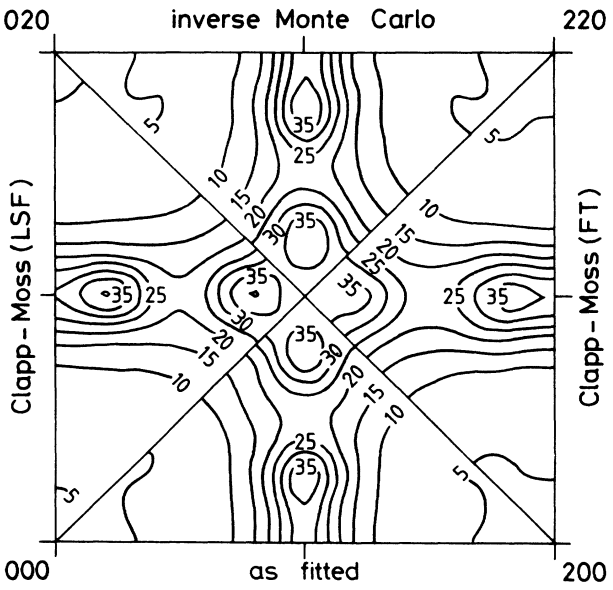

FIG. 5. Separated short-range order scattering $I_{SRO}(\mathbf{h})$ in 0.1 Laue units and recalculated intensities based on a Monte Carlo simulation and the effective pair potentials of Table V.

scattering,[26] but the effective pair potentials did not follow the Friedel scheme either.[17]

The dominance of V_{110} manifests itself via $\tilde{V}(\mathbf{Q})$ as streaked minima through $L1_2$-type superstructure positions along ⟨100⟩ directions, similar to the streaked maxima of I_{SRO} (Fig. 3). The weak modulation along the streaks means that $L1_2$-related superstructures with periodic antiphase boundaries, like DO_{22},DO_{23}, will not differ much in their energy of configuration.

The effective pair potentials of Table V were used to recalculate the short-range order scattering by the Monte Carlo method. The results are plotted in Fig. 5. In all cases the fourfold splitting is reproduced. The unweighted R values of the fits are 3.5 to 5.3% in comparison with I_{SRO} as separated.

V. A PROBABLE LOW-TEMPERATURE PHASE OF Cu_3Zn

At $T=0$ K, the ground state is determined by a minimum of the energy. Assuming no pronounced concentration dependence of the effective pair potentials, Table V can be used to obtain the energy difference between various ordered structures (with 25 at. % Zn) and a random arrangement of atoms. Based on the abundance of the Clapp configurations $C16$ and $C17$, the structures chosen were $L1_2$ ($M=\infty$), DO_{22} ($M=1$), DO_{23} ($M=2$), and an $L1_2$-based structure with a periodicity $M=3$ (for M, see Ref. 33). The results are summarized in Table VI. Only a small energy difference is found between these structures, mainly because α_{110} is always $-\frac{1}{3}$. Thus, the higher V_{lmn} are decisive in stabilizing DO_{23}. Increasing the number of potentials V_{lmn}, DO_{23} is typically the energetically favorable structure for lmn larger than 411. This is consistent with lattice energy considerations[34] leading to the condition that at least 10 V_{lmn} are needed for the stabilization of the DO_{23} structure.

TABLE VI. Energy difference per atom ΔE of various long-range ordered structures in comparison with a random Cu_3Zn alloy, using V_{lmn}^{IMC} of Table V.

Structure	ΔE (meV)
$L1_2$	−18.0
DO_{22}	−17.5
DO_{23}	−19.7
$L1_2, M=3$	−19.2

A DO_{23} structure might even be guessed from the $I_{SRO}(\mathbf{h})$ plot of Fig. 3. It is known that superstructure peaks appear at 100 positions for $L1_2$, at 100 and $1\frac{1}{2}0$ positions for DO_{22}, and at 100 and $1\frac{1}{4}0$ positions for DO_{23}. Figure 3 shows that whereas 100 and $1\frac{1}{2}0$ positions are saddle points, $1\frac{1}{4}0$ positions are close to the maxima in $I_{SRO}(\mathbf{h})$ [or to the minima in $\tilde{V}(\mathbf{h})$], thus favoring DO_{23} (the 100 superstructure reflection, always present in these structures, is energetically less favorably located).

The DO_{23} structure is also predicted by the Sato-Toth scheme[33] for structures with periodic antiphase boundaries. In this scheme, the valence-electron concentration per atom, e/a, the ratio t between the diameter of the actual Fermi surface along ⟨110⟩ directions and the one for a free-electron Fermi surface with the same e/a, and the periodicity M are interrelated according to

$$\frac{e}{a}=\frac{\pi}{12t^3}(2+M^{-1}+0.25M^{-2})^{1.5}\ .$$

With $e/a=1.25$ for Cu_3Zn and $t=0.94$ from the present measurements, one obtains $M=2.1$, close to the value of 2 for a DO_{23} structure. A DO_{23} structure has indeed been observed in Ag_3Mg and Au_3Cd, with $e/a=1.25$ in both cases.[35,36]

The critical temperature T_c for the order-disorder transition was estimated by a Monte Carlo simulation.[37] A model crystal consisting of a mixture of a DO_{23} ordered phase and a phase with a random atomic arrangement was used to reduce hysteresis effects. The order was characterized by introducing concentration waves.[38] For a DO_{23} structure, two long-range order parameters η_i are required, one for the wave vector (0,1,0) and another one for the wave vectors $(1,\frac{1}{4},0)$ and $(0,\frac{1}{4},1)$. Starting a simulation sequence from lower temperatures, at a value of ~ 0.75 for $\eta=(\eta_1+\eta_2)/2$, the stable low-temperature phase, DO_{23}, suddenly changed to the disordered state. A first-order character of this transition is expected from the phenomenological Landau theory, because the Lifshitz criterion[38] required for a continuous transition is violated: In the present case it is possible to construct a reciprocal lattice vector of the disordered phase as the sum of three vectors belonging to the stars[38] of the ordering wave vectors:

$$(0,1,0)+(1,\tfrac{1}{4},0)+(0,-\tfrac{1}{4},-1)=(1,1,-1)\ .$$

For the critical temperature a value of ~330 K was obtained.

In a forthcoming paper further results from samples with various compositions will be presented. They also support the low-temperature stability of the DO_{23} structure in Cu–25 at. % Zn.

[1]G. M. Stocks, M. Boring, D. M. Nicholson, F. J. Pinski, D. D. Johnson, J. S. Faulkner, and B. L. Gyorffy, in *Noble Metal Alloys,* Proceedings of the Metallurgical Society of AIME Annual Meeting, 1985, edited by T. B. Massalski, W. B. Pearson, L. H. Bennett, and Y. A. Chang (Metallurgical Society, Inc., Warrendale, PA, 1986), p. 27.

[2]J. Als-Nielsen, in *Phase Transitions and Critical Phenomena,* edited by C. Domb and M. S. Green (Academic, London, 1976), Vol. 5a, p. 87.

[3]A. Kussmann and H. Wollenberger, Z. Metallkd. **50**, 94 (1959).

[4]E. Balanzat and J. Hillairet, J. Phys. F **11**, 1977 (1981).

[5]W. Pfeiler, R. Reihsner, and D. Trattner, Scripta Metall. **19**, 199 (1985).

[6]M. Halbwachs, D. Beretz, and J. Hillairet, Acta Metall. **27**, 463 (1979).

[7]Th. Obenhuber, W. Adlassnig, U. Närger, J. Zänkert, W. Potzel, and G. M. Kalvius, Europhys. Lett. **3**, 989 (1987).

[8]D. T. Keating, Acta Metall. **2**, 885 (1954).

[9]B. E. Warren, *X-Ray Diffraction* (Addison-Wesley, Reading, 1969), p. 227.

[10]B. Borie and C. J. Sparks, Acta Crystallogr. Sect. A **27**, 198 (1971).

[11]G. Kostorz, in *Physical Metallurgy,* edited by R. W. Cahn and P. Haasen (North-Holland, Amsterdam, 1983), p. 793.

[12]L. H. Schwartz and J. B. Cohen, *Diffraction from Materials* (Springer, Berlin, 1987), p. 402.

[13]P. P. Müller, B. Schönfeld, G. Kostorz, and W. Bührer, Acta Metall. **37**, 2125 (1989).

[14]D. de Fontaine, Acta Metall. **23**, 553 (1975).

[15]P. C. Clapp and S. C. Moss, Phys. Rev. **142**, 418 (1966).

[16]B. Schönfeld, L. Reinhard, G. Kostorz, and W. Bührer, Phys. Status Solidi B **148**, 457 (1988).

[17]V. Gerold and J. Kern, Acta Metall. **35**, 393 (1987).

[18]V. F. Sears, Atomic Energy of Canada Ltd. Report No. AECL-8490, 1984 (unpublished).

[19]M. W. Johnson, United Kingdom Atomic Energy Authority—Atomic Energy Research Establishment Report No. AERE-R7682, 1974 (unpublished).

[20]R. Colella and B. W. Batterman, Phys. Rev. B **1**, 3913 (1970).

[21]S. L. Quimby and P. M. Sutton, Phys. Rev. **91**, 1122 (1953).

[22]J. A. Rayne, Phys. Rev. **112**, 1125 (1958).

[23]S. C. Moss, Phys. Rev. Lett. **22**, 1108 (1969).

[24]K. Ohshima, J. Harada, and S. C. Moss, J. Appl. Crystallogr. **19**, 276 (1986).

[25]K. Ohshima and D. Watanabe, Acta Crystallogr. Sect. A **29**, 520 (1973).

[26]R. O. Scattergood, S. C. Moss, and M. B. Bever, Acta Metall. **18**, 1087 (1970).

[27]M. Haghgooie, S. Berko, and U. Mizutani, in *Proceedings of the Fifth International Conference on Positron Annihilation, Lake Yamanaka, Japan, 1979,* edited by R. R. Hasiguti and K. Fujirawa (Japan Institute of Metals, Sendai, 1979), p. 291.

[28]R. Prasad, S. C. Papadopoulos, and A. Bansil, Phys. Rev. B **23**, 2607 (1981).

[29]R. O. Williams, Oak Ridge National Laboratory Report No. ORNL-4828, 1972 (unpublished).

[30]H. Suzuki, J. Harada, T. Nakashima, and K. Adachi, Acta Crystallogr. Sect. A **38**, 522 (1982).

[31]P. C. Clapp, Phys. Rev. B **4**, 255 (1971).

[32]J. Friedel, Nuovo Cimento (Suppl.) **2**, 287 (1958).

[33]H. Sato and R. S. Toth, Phys. Rev. **124**, 1833 (1961).

[34]J. Kanamori and Y. Kakehashi, J. Phys. (Paris) Colloq. **38**, C7-274 (1977).

[35]K. Schubert, B. Kiefer, M. Wilkens, and R. Haufler, Z. Metallkd. **46**, 692 (1955).

[36]M. Hirabayashi and S. Ogawa, Acta Metall. **9**, 264 (1961).

[37]K. Binder, in *Monte Carlo Methods in Statistical Physics,* edited by K. Binder (Springer, Berlin, 1979), p. 1.

[38]A. G. Khachaturyan, Prog. Mater. Sci. **22**, 1 (1978).